MANUSCRIPT

Tuning Hydrogen Bond Networks at Gold Electrodes: A Study of Potential-Dependent DMSO-Water Interfaces

Ziareena A. Al-Mualem[1], Alfredo E. Cardenas[2], Sulagna Hazarika[1], Hang Ren[1], Carlos R. Baiz[1,*]

[1]Department of Chemistry, University of Texas at Austin, 105 E 24th St. A5300, Austin, TX 78712, USA

[2]The Oden Institute for Computational Engineering and Sciences, University of Texas at Austin, 105 E 24th St. A5300, Austin, TX 78712, USA

*Corresponding author: cbaiz@cm.utexas.edu

Keywords

SEIRAS, molecular dynamics, hydrogen bonds, cosolvents, electrochemistry, interfaces

Abstract

Understanding the behavior of hydrogen bond (H-bond) networks at electrode interfaces is the first step towards optimizing electrochemical processes. This study investigates the potential-dependent interfacial environment of dimethyl sulfoxide (DMSO)−water mixtures at gold electrodes using a combination of surface-enhanced infrared absorption spectroscopy (SEIRAS) and constant-potential molecular dynamics (MD) simulations. SEIRAS provides *in situ* spectroscopic data on H-bonding populations and cosolvent enrichment at the interface, while MD simulations offer an atomistic view of H-bond configurations and molecular orientations under applied potentials. Our results demonstrate that applied electrostatic potential influences the interfacial H-bonding environment. Negative potentials produce enrichment of DMSO and a reorientation of interfacial water molecules, which leads to a slight increase in H-bonded populations, particularly at lower DMSO concentrations. Conversely, positive potentials show a reduced impact on the H-bond structure. The effects are different at higher DMSO concentrations

where DMSO–DMSO interactions dominate. Despite DMSO being electrically neutral, both experimental and simulation data reveal a measurable modulation of interfacial enrichment and H-bond populations as a function of potential.

1. Introduction

The interface between metal surfaces and solutions presents a complex chemical environment. Interfacial regions are often increasingly reactive compared to bulk solutions facilitating catalytic reactions. Additionally, molecules or ions can adsorb onto the metal surface, thereby altering the concentration of species in both the solution and on the metal surface and altering the energetics and kinetics of electrocatalytic reactions at the electrode-electrolyte interface. In aqueous solutions, water often serves as both a reactant and a solvent, influencing reactions such as the hydrogen evolution reaction (HER), oxygen reduction reaction, and the CO_2 reduction reaction.(1–3) Understanding the role of interfacial water structure is essential for advancing the understanding of electrocatalytic processes in aqueous media.

The mechanism of HER involves proton-coupled electron transfer to form adsorbed H as the key intermediate, with either H_3O^+ or H_2O as the proton source. In HER, the cathodic half of water splitting by electrolysis, aprotic solvents can tune water-water H-bonds in solution.(1) Since HER under neutral and alkaline conditions relies on water as both a reactant and solvent, optimizing this reaction requires control of the water network at the cathode interface. One promising approach to tune the HER reactivity involves the addition of a cosolvent, which can modulate the hydrogen-bonding environment.(4) The polarity, high water-miscibility, donor-acceptor imbalance, and amphiphilic behavior of dimethyl sulfoxide (DMSO), make DMSO–water cosolvent systems a promising approach to control the local interfacial environment and water network,(5) potentially controlling kinetics and transport in electrocatalytic reactions. DMSO disrupts its local H-bonding environment by accepting up to two H-bonds with nearby water molecules, as well as forming DMSO dimers by hydrophobic interactions through its methyl

groups. These interactions produce microscopic liquid-liquid phase separation that lead to heterogeneous regions enriched in DMSO and regions enriched in water, producing microscopic percolated H-bond networks(6, 7) and concentration-dependent solvation dynamics in aqueous systems.(8–14) (9, 15, 16)

We have previously shown that DMSO alters the interfacial hydration environment on gold surfaces.(5) Interfacial DMSO molecules are dehydrated and enriched on the Au surface, accompanied by the formation of small water clusters form on the surface. Simulations show a "buckled" conformation of water molecules at the Au surface. This energetically-unfavorable conformation, along with the small cluster sizes, inhibits H-bonding with bulk water, potentially restricting the proton diffusion and transfer necessary for HER. While these recent studies revealed important details about the effects of DMSO, it is necessary to further characterize cosolvent effects under applied electrochemical potentials to further understand how interfaces change as potentials approach *in operando* conditions. Specifically, here we aim to understand the effects of applied surface potentials on interfacial DMSO or water enrichment and depletion as well as characterize how the applied potential alters DMSO and water configurations at the gold interface.

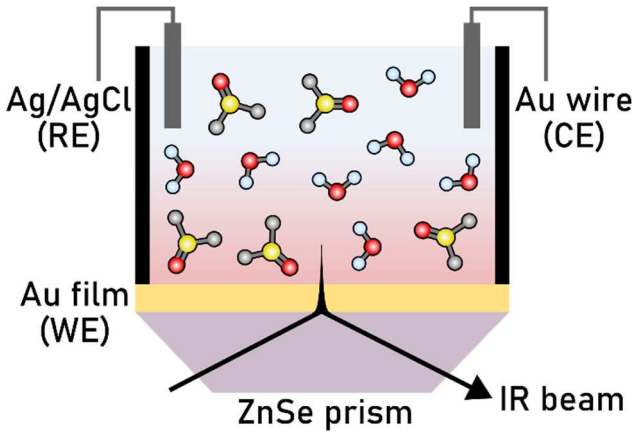

Figure 1. Illustration of the SEIRAS setup for *in situ* spectroelectrochemical measurements of the cosolvent systems. The reference electrode (RE) and counter electrode (CE) are Ag/AgCl and a gold wire, respectively. The gold film is the working electrode (WE). The ZnSe prism is the ATR substrate.

This study employs a combination of *in situ* experimental spectroelectrochemical measurements using surface-enhanced infrared absorption spectroscopy (SEIRAS) and molecular dynamics (MD) simulations to investigate the local H-bonding networks in water−DMSO cosolvent mixtures on gold electrodes under a range of applied electrostatic potentials. SEIRAS measures interfacial molecular structure and reactions as detection sensitivity is greatly enhanced at metal-liquid interfaces without interference from the bulk phase.(17–20) In SEIRAS, a nanoscale-roughened thin metal film is deposited onto an attenuated total reflectance (ATR) crystal; this metal film serves as the working electrode in electrochemical experiments.(20) The incoming IR beam excites local surface plasmons in the metal film, resulting in a near-field enhancement with a penetration depth of ~100 nm into the sample. The solvent absorption is minimized from the rapid decay in the enhancement penetration.(21, 22) SEIRAS provides an ensemble-averaged view of the system, while MD simulations provide a localized atomistic picture of the water network structure and geometry at the metal-liquid interface.

2. Methods

Cosolvent Sample Preparation

DMSO–water cosolvent mixtures were prepared for SEIRAS by titrating appropriate volumes of DMSO (≥99.9%, anhydrous; Sigma-Aldrich) into a solution of ultrapure water (Milli-Q) and 20 mol% D_2O (99.9%; Cambridge Isotope Laboratories, Inc.) during the measurements. The mixture compositions were: 0 (no DMSO), 1, 3, 5, 7, 10, 15, 20, 25, 30, 35, and 40 mol% DMSO. The electrolyte was 10 mM $KClO_4$ in ultrapure water. Perchlorate (ClO_4^-) was chosen as it weakly adsorbs on gold.(23, 24) The electrolyte concentration was maintained across all samples.

Gold Surface Preparation for SEIRAS

The gold surface for SEIRAS measurements was prepared using a modified electroless deposition procedure described previously.(5) A ZnSe ATR prism (60° cut; Pike Technologies) was polished with 1 µm and 0.05 µm alumina slurry then sonicated in ultrapure water for 10 minutes. The ZnSe crystal was then heated to 50° C and 200 µL of a 25 mM solution of gold(III) chloride trihydrate ($HAuCl_4•3H_2O$) (99.9+%; Sigma-Aldrich) in ultrapure water was dropcasted onto the crystal face and left to deposit for 3 minutes; this deposition time results in a thicker gold film with an enhancement penetration depth under 70 nm.(5) The surface was rinsed with water to quench the deposition then dried with a gentle flow of nitrogen gas. The gold surface resistance was 0.9 Ω across a ~1 cm distance on the crystal face.

Spectroelectrochemical Measurements

SEIRAS measurements were conducted with a Bruker INVENIO Spectrometer equipped with a liquid-nitrogen-cooled mercury-cadmium-telluride (MCT) detector and a Pike Technologies VeeMAX III accessory with the Jackfish J2F electrochemical cell. The Ag/AgCl reference electrode was filled with 3 M KCl. A gold wire was used as the counter electrode. A custom-built

LabVIEW data acquisition program was used to synchronize applying a potential with a CH Instruments 1202C potentiostat through the Hard Potato package(25) and collecting the corresponding IR spectra. Prior to data acquisition, the gold surface and electrodes were cleaned in a 10 mM $KClO_4$ in ultrapure water electrolyte solution with >20 CV cycles from -0.8 V to 0.7 V with a 0.1 V/s scan rate (**Figure S47**). The set potentials (-0.6 V to 0.6 V in steps of 0.1 V) were corrected relative to the open circuit potential (OCP) measured at the beginning of the experiment. Each spectrum was averaged from 128 scans with a 2 cm^{-1} spectral resolution. The 10 mM $KClO_4$ electrolyte solution was used as the background to solvent-correct the spectra. All spectra were collected at room temperature under a purge of dry air.

Molecular Dynamics Simulations

Mixtures of 1%, 5%, 10%, and 20% DMSO in water in between two gold electrodes were prepared using the CHARMM-GUI Multicomponent Assembler module.(26–29) Each gold electrode consisted of three layers of (111) faces (624 Au atoms in each electrode). The two electrodes were placed parallel to each other, and perpendicular to the z-axis. The initial separation between the electrodes was 10 nm (the separation varied during the equilibration steps) and their dimensions in the x- and y-directions were 3.75 nm and 4.00 nm, respectively. CHARMM36 force field parameters(30) were used for DMSO and a TIP3P model(31) was used for water molecules. The gold atoms were modeled with the Interface force field(32) that is compatible with CHARMM. In addition to setting up this set of systems with parallel electrodes, aqueous systems with the same DMSO and water compositions were also prepared but without the gold electrodes. For the latter, standard NPT simulations at 300 K and 1 atm were performed to obtain the mixtures' densities.

MD simulations for the electrode systems were performed with the LAMMPS software package (version 2Aug2023)(33) along with the ELECTRODE package(34) in LAMMPS that implements a constant potential method. During minimization and equilibration, periodic boundary conditions were used in the x- and y-directions and non-periodic boundary conditions in the z-direction, for which the slab method(35) was applied with a correction factor of 3.0. For each prepared system, a short minimization using a conjugate gradient algorithm was followed by a 2-ns equilibration run where we turn on the constant potential algorithm. In these equilibration runs, one electrode was fixed and the second electrode was allowed to move like a rigid piston along the z-direction under the influence of an external pressure of 1 atm. Temperature was maintained at 300 K using a Nosé-Hoover thermostat.(36) For each mixture, two sets of simulations were performed: **1.** The electrode potential was kept at 0 V for both electrodes and **2.** One electrode was set at -0.6 V and the other at 0.6 V. For the equilibration runs, a conjugate gradient minimization algorithm (that allows moving electrodes) was used to obtain the electrode charge at every time step.(37) At the end of these runs we verified that the bulk densities at the center of the simulation box were like the bulk densities obtained in the NPT runs of the same DMSO/water mixtures (with no electrodes) mentioned above. Finally, 12-ns production runs were performed with fixed electrode locations using periodic boundary conditions in all spatial directions using the finite field approach(38, 39) as implemented in the ELECTRODE package in LAMMPS. A 2-fs time step was used for equilibration and production runs using SHAKE(40) to constrain molecular bonds. Configurations were saved every 2 ps for analysis. Van der Waals interactions were modeled with Lennard-Jones potentials using a 1.2 nm cutoff and the long-range electrostatics interactions were computed with a particle-particle-particle-mesh method(41) with relative accuracy of 10^{-7}. For some of the analysis reported here we used analysis tools from GROMACS software.(42)

3. Results and Discussion

Interfacial H-Bonding Environment from Experiment

The S=O stretching region reveals the balance of DMSO–water and DMSO–DMSO interactions at the interface. Quantitative analysis to extract the DMSO H-bonded and non-bonded populations was performed via a global fitting algorithm of the experimental spectra.(5, 6) This procedure fits the spectra to six Gaussian functions that correspond to six distinct populations with the following center frequencies: 2HB at 1009 cm^{-1}, 1HB at 1022 cm^{-1}, 0HB at 1058 cm^{-1}, aggregate at 1040 cm^{-1}, -CH_3 rocking at 1016 cm^{-1}, and aggregate -CH_3 rocking at 1034 cm^{-1}. The relative population of each species can be calculated as the ratio of the oscillator-strength corrected areas of each fitted Gaussian profile relative to the total peak areas (excluding the overlapping -CH_3 rocking mode). The global fitting procedure is described in detail in **Section S2**.

We have previously reported the concentration-dependent changes at the interface in comparison to the bulk at OCP. In brief, we showed that DMSO is enriched by a factor of ~4× at the interface compared to the bulk at low DMSO concentration.(5) In addition, the number of S=O–water H-bonds was reduced at the interface compared to bulk, which points towards the interface being a significantly more hydrophobic environment than the bulk. Here, we focus on the effects of applied potential on the local interfacial environment. The changes in lineshapes are relatively small, though the changes can be observed when computing the difference across different potentials (**Figure 2**, **Figures S4-5**). The effect of potential is more pronounced at low concentrations. At negative potentials, the S=O stretch exhibits a minor redshift in center frequency and a higher absorbance. This redshift is more prominent in lower DMSO concentrations and can be attributed to a population increase of more hydrated DMSO molecules

at the interface. Conversely, at positive potentials, the S=O stretch appears similar to 0 V at concentrations below 25 mol% DMSO (**Figure S4**). The full-width at half-maximum values increase with increasing concentration but not with applied potentials (**Figure S5**).

The H-bond analysis for the S=O group (**Figure 3**), obtained by fitting the lineshapes, as described above, reveals that the H-bond populations are dependent on the potential. The potential-dependent H-bond populations can be interpreted within three different concentration regimes, despite the error bars being relatively large, trends can nonetheless be observed: **1.** At low concentrations (<10 mol%), negative potentials increase the number of H-bonds at the interface. However, positive potentials (above 0 V) are observed to have only a slight effect on the H-bond populations (**Figure 3A-C**). **2.** Within the intermediate concentration range (15-30 mol%) there is effectively no change in the number of H-bonds (**Figure 3D**). **3.** In the high concentration range (>30 mol%), we observe that the trend is reversed compared to the dilute regime, in this case there is a slight decrease in the number of H-bonds at negative potentials (**Figure 3E**). These non-monotonic trends with voltage and concentrations point towards multiple phenomena contributing to changes in the local environment at the interface.

Next we examine interfacial water by measuring the O–D stretching mode of HOD in H_2O (or the O–H stretching mode of HOD in D_2O), which provides direct molecular information on the H-bonding environment of water.(43, 44) **Figure S6** shows an increase in the O–D stretch absorbance below 10 mol% DMSO at positive potentials. After normalization, the lineshapes show negligible changes from applied potentials (**Figure S7**). These results indicate that the H-bond

populations of water remain unchanged as a function of potential, perhaps suggesting that DMSO plays a more important role in modulating the interfacial environment.

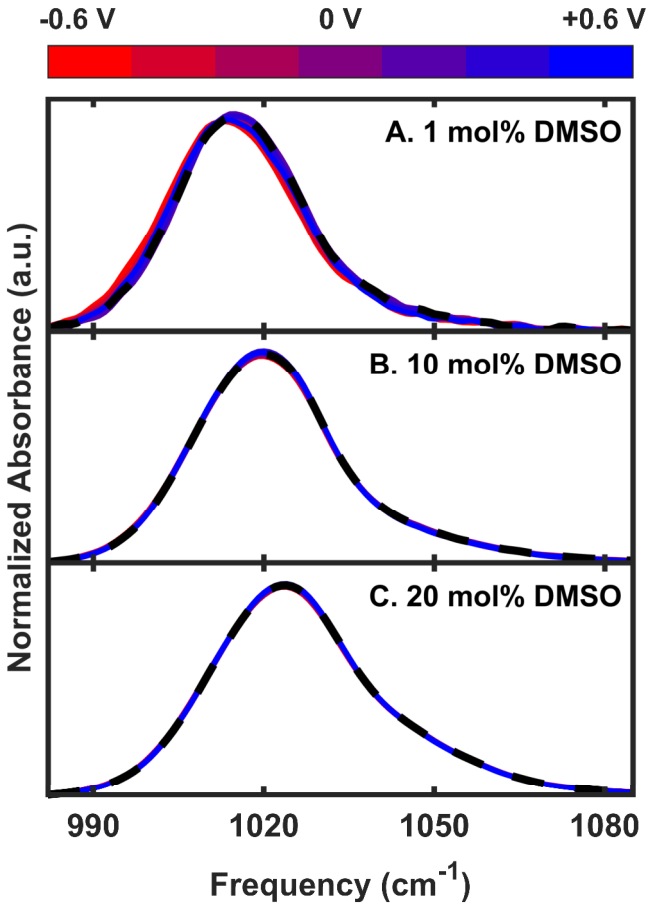

Figure 2. Representative SEIRAS spectra of the S=O stretching region at (A) 1 mol% DMSO, (B) 10 mol% DMSO, and (C) 20 mol% DMSO, at select applied potentials (from -0.6 V, red, to +0.6 V, blue, in steps of 0.2 V) and at 0 V potential (black dashed line). Spectra were normalized by total peak area. Additional spectra at all measured concentrations and applied potentials can be found in **Figure S2**.

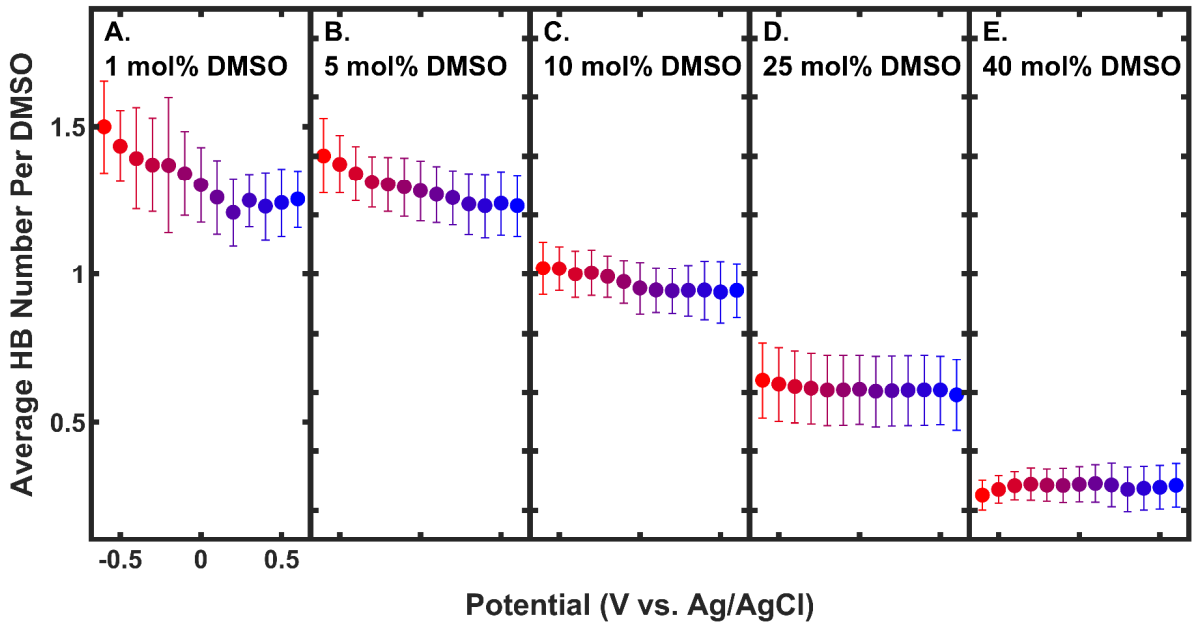

Figure 3. Average H-bonding (HB) number per DMSO molecule at the gold electrode as a function of applied potential (-0.6 V in red to +0.6 V in blue) at select dilute (1, 5, 10 mol% DMSO, panels A-C) and concentrated (25, 40 mol% DMSO, panels D-E) compositions. The error bars represent standard deviation calculated from the global fitting procedure. Additional spectra at all measured concentrations and applied potentials can be found in **Figure S8**.

Potential-Dependent Enrichment of Interfacial Molecules

The potential-dependent interfacial enrichment or depletion of DMSO and water be computed from the experimental spectra by taking the ratio of integrated peak areas before normalization (relative to 0 V potential): a relative enrichment value > 1 means a larger IR absorbance, or "enrichment", and a value < 1 means a lower IR absorbance, or "depletion". **Figure 4A** shows a general enrichment of DMSO at more negative potentials by at least 5% compared to 0 V at all DMSO concentrations. At 1 mol% DMSO, the largest DMSO relative enrichment is ~8%, then increases at 3 mol% to ~13%, and plateaus starting from 20 mol% to ~5%. At positive applied potentials, the only DMSO relative depletion over 5% is ~14% at 1 mol% DMSO. On the other hand, water is enriched at more negative potentials (-0.6 V) and only at concentrations below

10 mol% DMSO (**Figure 4B**), with highest enrichment ~17% at 0 mol%. Water does not exhibit any interfacial depletion with applied potential below 30 mol%.

One possible interpretation for an increase in IR absorbance (or enrichment) with an applied potential is an increase in the population of that specific species at the interface. Another possible explanation for the changes in IR signal is molecular reorientation in the interfacial region. SEIRAS is a surface-sensitive and orientation-selective technique. In SEIRAS, oscillators with transition dipoles perpendicular to the enhanced field are more SEIRAS-active and contribute the largest spectroscopic signal.(45) However, both the change in population and molecular reorientation could be concurrent with applied potential. While the effects of potential are relatively modest, showing a ~10% modulation of the signal, with most pronounced changes at the lowest concentrations, these changes are relatively small compared to the overall enrichment effects of concentration, which in DMSO we observed to be 200-400% enrichment at the surface. Nonetheless, this study shows that changes in potential can affect the interface, despite species being uncharged.

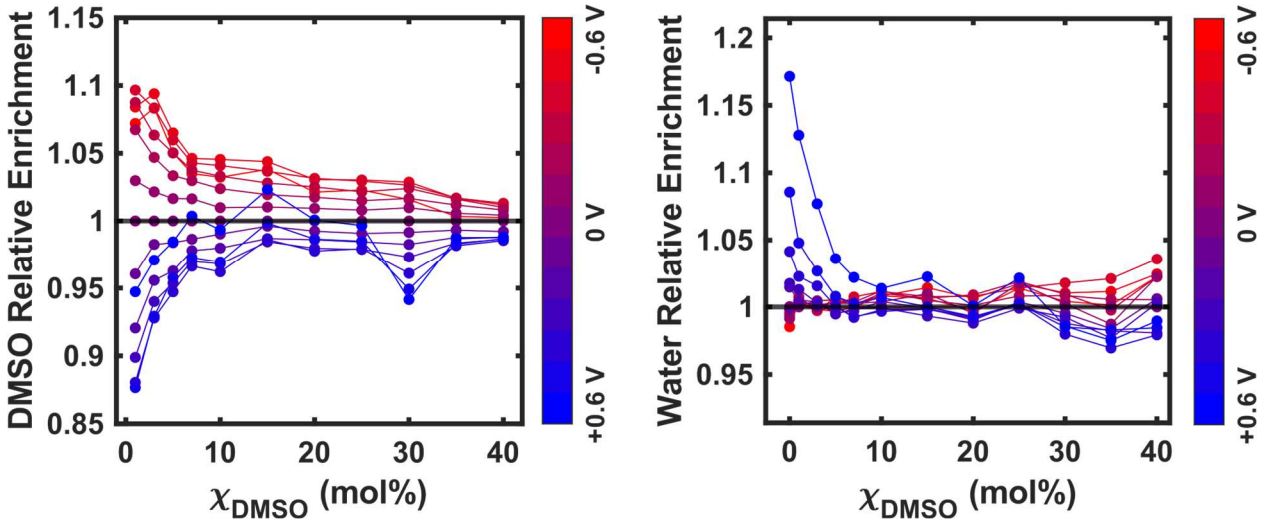

Figure 4. Relative enrichment of (A) DMSO and (B) water at the gold electrode at applied potentials (-0.6 V in bright red to +0.6 V in bright blue) as a function of DMSO mol% compared to 0 V potential conditions. The potential values are relative to the Ag/AgCl reference electrode. The enrichment was calculated as the ratio of the peak area at applied potentials to the peak area without an applied potential. Note: the DMSO mol% values in (A) and (B) start at 1 mol% and 0 mol%, respectively.

Interpretation of interfacial interactions from constant-potential MD simulations

Spectroscopic observations suggest that voltage modulates the interfacial H-bond networks, whether by changing the ratios of DMSO and water, or by altering molecular configurations, such as orientations. We interpret these changes by performing constant-potential MD simulations. In these simulations, the gold atoms are assigned initial charges, which are then re-optimized throughout the simulation as the liquid reorganizes around the surface. This enables the surface to "respond" to changes in the cosolvent molecules, in order to maintain a constant potential. Simulations are carried out at three different potentials, 0 V, -0.6 V and +0.6 V, thus enabling us to compare the results extracted from MD trajectories with experimental observables. A snapshot of the MD box is included in **Figure S32**

H-bond populations, computed from MD simulations (**Figure 5**), show the differences between the bulk and the interfacial environments, as well as the effect of potential on the relative

populations at the interface. The changes in bulk vs interface can be compared with previous results under open circuit potential. Qualitatively, the current MD simulations are consistent with previous results, showing dehydration at the interface, the H-bond populations are consistent with previous experiments and MD simulations.(5) This is expected, given that the MD force fields were the same as the previous simulations. The key difference is that the present MD simulations are constant-potential MD simulations, with fluctuating charges on the gold atoms, compared to previous simulations without charges on the gold atoms.(5) The constant-potential MD simulations account for electrode polarization, and thus are expected to more accurately reproduce the environment at the interface.

The effects of potential on H-bond populations can be observed by comparing the MD trajectories for positive, neutral, and negative potentials (**Figure 5**). The effect of potential on H-bond populations is relatively small compared to the populations in bulk versus surface, nonetheless the simulation results are consistent with experiment: simulations show that at low DMSO concentrations (1 mol%), negative potentials increase the number of hydrogen bonds compared to positive potentials. Higher concentrations (20 mol%) show an increase in the number of H-bonds at positive potentials. Interestingly, simulations also exhibit non-monotonic trends where the effect at 5 mol% shows an increase.

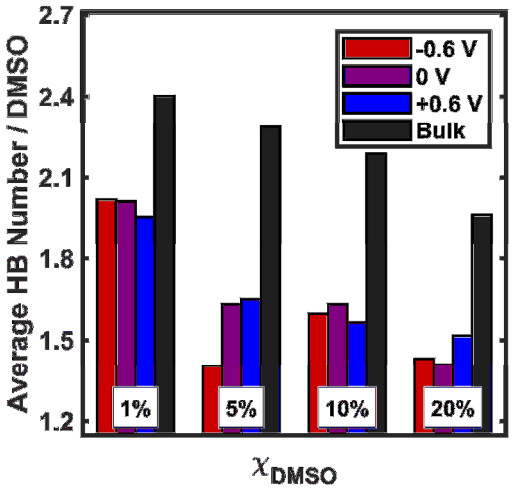

Figure 5. Average H-bonding (HB) number per DMSO molecule as a function of DMSO mol% at applied potentials and bulk from MD simulations. The black bars represent the average number of H-bonds in bulk, and the (red, purple, and blue) bars represent interfacial populations at -0.6, 0, and 0.6 V respectively. For the applied potential systems, the error estimates by block averaging are < 0.05 (in units of HB numbers) for the 1% and 5% mixtures and < 0.2 for the 10% and 20% mixtures. For the HB numbers in the bulk the errors are < 0.001.

The enrichment at the interface (Figure 6) is significantly greater compared to experiments, with simulations showing a ~12× enrichment versus the bulk and experiments showing a ~4× enrichment at the lowest DMSO concentrations (5). This means that when the bulk concentration is 1 mol% DMSO, experiments predict that the interface contains 4 mol% DMSO, and simulations show a 12 mol% DMSO concentration. As observed from H-bond populations in bulk experiments, this change in concentration can lead to significant changes in H-bond populations. In addition, we can examine the effects of potential on the molecular orientations at the interface. **Figures S33-36** show the average dipole orientations computed of water as a function of distance from the electrode surface for positive, neutral, and negative interfaces, across DMSO concentrations. In addition, **Figures S37-38** show the orientation of DMSO molecules. Generally, we observe that potential does not significantly impact the orientations of DMSO, however, water orientations are significantly altered as a result of applied potential. Without potential, the net orientation is perpendicular to the surface, as discussed in previously where water molecules are

observed to assume a "buckled" configuration(5). Once the potential is turned on, strong preferential orientation is observed throughout the box. Near the surface, at negative potential we observe particularly strong reorientation across all DMSO concentrations. For instance, at 1% the dipole projection in pure water is approximately 0, and this value increases to ~0.3 indicating that on average the water molecules adopt an angle of ~73° suggesting that the HER process could be significantly altered given the strong reorientation of water near the interface. Positive potential does not appear to reorient water as strongly. This is consistent with the effects on H-bond populations (**Figure 3**), where positive potentials appear to have a more moderate effect compared to negative potentials.

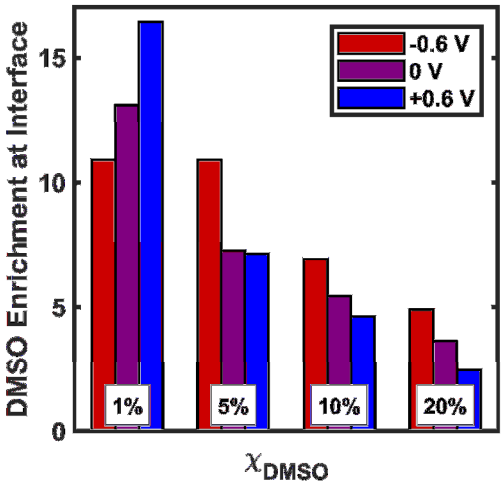

Figure 6. DMSO enrichment at the gold electrode at applied potentials (0 V in purple, -0.6 V in red, +0.6 V in blue) as a function of DMSO mol% from MD simulations. Error estimates obtained by block averaging are smaller than 0.8.

Overall, MD simulations are consistent with SEIRAS measurements, showing that the effect of potential on enrichment is relatively moderate, and that the strongest effects are related to the dipole orientations. The non-monotonic changes in H-bond populations across DMSO

concentrations are also consistent between experiment and simulation. We have identified the most important factors that drive changes in H-bond populations, namely the enrichment of DMSO and reorientation of water molecules.

4. Conclusions and Outlook

In summary, SEIRAS reveals that concentration and potential-dependent changes in the S=O H-bond populations decrease slightly as the potential becomes more positive. The extent of this decrease varies depending on the DMSO concentration. At lower concentrations and negative potentials, the hydrogen bonding is more pronounced, possibly due to fewer DMSO–DMSO interactions and more DMSO–water interactions as well as a stronger effect of potential on water reorientation. Furthermore, within negative potentials, DMSO molecules show significant enrichment at the gold electrode surface. At low concentrations (e.g., 1 mol%), DMSO enriches up to ~8%. As the concentration increases from 3 mol% to 20 mol%, enrichment peaks around 13% before stabilizing, suggesting surface saturation. This is because, at more negative potentials, the surface of the gold electrode is likely more electron-rich, which could lead to stronger interactions between the electrode and solvent molecules. These stronger interactions disrupt the interfacial H-bond networks, potentially decreasing the average H-bond number. Within the higher concentration regime, the average H-bond number becomes less dependent on the applied potentials, indicating that the system becomes less sensitive to changes in the potential, possibly because water becomes a smaller component, and changes in orientation are less pronounced. Within the high concentration regime, DMSO–DMSO interactions dominate, and the average number of H-bonds per DMSO molecule is lower and relatively constant across the applied potential range. The stabilization seen here suggests that the H-bonding network reaches a limit

where additional DMSO molecules do not significantly change the overall hydrogen bonding environment.

Above 20 mol%, enrichment reaches ~5%, indicating a balanced distribution between DMSO and water. This enrichment of DMSO at the negatively charged surface (Figures S43-S44) is likely due to the electrostatic interactions between the polar DMSO molecules and the negatively charged electrode. DMSO has a large dipole moment, with a partial positive charge on the sulfur atom and partial negative charges on the oxygen atoms. This polarity makes DMSO molecules more likely to align with the negatively charged surface. At positive potentials (+0.6 V), there is a depletion of DMSO at the interface, particularly at low concentrations (~14% depletion at 1 mol%). As concentration increases, depletion lessens, though some DMSO remains at higher concentrations (Figures S39-S42). This is likely due to repulsion from the positively charged surface, causing DMSO displacement.

In conclusion, we have characterized the H-bond populations and enrichment of water and DMSO across a range of potentials and concentrations. The results show that the effect of potential is relatively small compared to the overall differences between the surface and bulk, nonetheless, the negative potentials modulate the H-bond populations, and we have observed that despite cosolvents being electrically neutral there is a measurable potential-dependent enrichment/depletion of cosolvents at the surface. These studies provide a foundation for understanding electrochemical catalysis in water such as the HER or CO_2 reduction reaction. In general, characterizing the H-bond networks provides a more complete picture for incorporating these effects into modeling and optimizing electrocatalytic processes at the interface. The present

studies provide an initial characterization of interfacial H-bond ensembles, further studies will incorporate dynamics, measuring the effects of potential on the lifetimes of H-bond at the interface.

Data Availability Statement: The data supporting this article have been included as part of the Supplementary Information.

ACKNOWLEDGEMENTS

This project was funded by the U.S. Department of Energy (DE-SC0023221) and the Welch Foundation (F-1891 to C.R.B. and F-2158 to H.R.). C.R.B. thanks the Alfred P. Sloan Foundation for their support. Z.A.A. was funded by a UT Austin Provost's Graduate Excellence Fellowship. Part of the simulations were carried out at the Texas Advanced Computing Center (TACC). The authors thank Keegan Lorenz-Ochoa for insightful discussions.

References

1. Gomes, R.J., R. Kumar, H. Fejzić, B. Sarkar, I. Roy, and C.V. Amanchukwu. 2024. Modulating water hydrogen bonding within a non-aqueous environment controls its reactivity in electrochemical transformations. *Nat. Catal.* 7:689–701.

2. Dubouis, N., A. Serva, R. Berthin, G. Jeanmairet, B. Porcheron, E. Salager, M. Salanne, and A. Grimaud. 2020. Tuning water reduction through controlled nanoconfinement within an organic liquid matrix. *Nat. Catal.* 3:656–663.

3. Wang, T., Y. Zhang, B. Huang, B. Cai, R.R. Rao, L. Giordano, S.-G. Sun, and Y. Shao-Horn. 2021. Enhancing oxygen reduction electrocatalysis by tuning interfacial hydrogen bonds. *Nat. Catal.* 4:753–762.

4. Xu, K. 2004. Nonaqueous liquid electrolytes for lithium-based rechargeable batteries. *Chem. Rev.* 104:4303–4417.

5. Al-Mualem, Z.A., K.A. Lorenz-Ochoa, L. Pan, H. Ren, and C.R. Baiz. 2024. Controlling Interfacial Hydrogen Bonding at a Gold Surface: The Effect of Organic Cosolvents. *J. Phys. Chem. Lett.* 15:4391–4399.

6. Oh, K.-I., K. Rajesh, J.F. Stanton, and C.R. Baiz. 2017. Quantifying hydrogen-bond populations in DMSO/water mixtures. *Angew. Chem. Int. Ed. Engl.* 129:11533–11537.

7. Scherer, J.R., M.K. Go, and S. Kint. 1973. Raman spectra and structure of water in dimethyl sulfoxide. *J. Phys. Chem.* 77:2108–2117.

8. Harpham, M.R., N.E. Levinger, and B.M. Ladanyi. 2008. An investigation of water dynamics in binary mixtures of water and dimethyl sulfoxide. *J. Phys. Chem. B*. 112:283–293.

9. Oh, K.I., X. You, J.C. Flanagan, and C.R. Baiz. 2020. Liquid-Liquid Phase Separation Produces Fast H-Bond Dynamics in DMSO-Water Mixtures. *J. Phys. Chem. Lett.* 11:1903–1908.

10. Wong, D.B., K.P. Sokolowsky, M.I. El-Barghouthi, E.E. Fenn, C.H. Giammanco, A.L. Sturlaugson, and M.D. Fayer. 2012. Water dynamics in water/DMSO binary mixtures. *J. Phys. Chem. B*. 116:5479–5490.

11. Banik, D., N. Kundu, J. Kuchlyan, A. Roy, C. Banerjee, S. Ghosh, and N. Sarkar. 2015. Picosecond solvation dynamics - A potential viewer of DMSO - Water binary mixtures. *J. Chem. Phys.* 142.

12. Lotze, S., C.C.M. Groot, C. Vennehaug, and H.J. Bakker. 2015. Femtosecond mid-infrared study of the dynamics of water molecules in water-acetone and water-dimethyl sulfoxide mixtures. *J. Phys. Chem. B*. 119:5228–5239.

13. Hazra, M.K., and B. Bagchi. 2018. Non-equilibrium solvation dynamics in water-DMSO binary mixture: Composition dependence of non-linear relaxation. *J. Chem. Phys.* 149.

14. Luzar, A., and D. Chandler. 1993. Structure and hydrogen bond dynamics of water–dimethyl sulfoxide mixtures by computer simulations. *J. Chem. Phys.* 98:8160–8173.

15. Perera, A., and R. Mazighi. 2015. On the nature of the molecular ordering of water in aqueous DMSO mixtures. *J. Chem. Phys.* 143.

16. Oh, K.-I., and C.R. Baiz. 2020. Molecular heterogeneity in aqueous cosolvent systems. *J. Chem. Phys.* 152:190901.

17. Ataka, K.I., and M. Osawa. 1998. In situ infrared study of water-sulfate coadsorption on gold(111) in sulfuric acid solutions. *Langmuir*. 14:951–959.

18. Aguirre, A., C.L.A. Berli, and S.E. Collins. 2017. ATR-FTIR spectrokinetic analysis of the CO adsorption and oxidation at water/platinum interface. *Catal. Today*. 283:127–133.

19. Kas, R., O. Ayemoba, N.J. Firet, J. Middelkoop, W.A. Smith, and A. Cuesta. 2019. In-Situ Infrared Spectroscopy Applied to the Study of the Electrocatalytic Reduction of CO2: Theory, Practice and Challenges. *ChemPhysChem*. 20:2904–2925.

20. Delley, M.F., E.M. Nichols, and J.M. Mayer. 2021. Interfacial Acid-Base Equilibria and Electric Fields Concurrently Probed by in Situ Surface-Enhanced Infrared Spectroscopy. *J. Am. Chem. Soc.* 143:10778–10792.

21. Ataka, K., T. Kottke, and J. Heberle. 2010. Thinner, smaller, faster: IR techniques to probe the functionality of biological and biomimetic systems. *Angew. Chem. - Int. Ed.* 49:5416–5424.

22. Kozuch, J., K. Ataka, and J. Heberle. 2023. Surface-enhanced infrared absorption spectroscopy. *Nat. Rev. Methods Primer 2023 31*. 3:1–19.

23. Angerstein-Kozlowska, H., B.E. Conway, A. Hamelin, and L. Stoicoviciu. 1987. Elementary steps of electrochemical oxidation of single-crystal planes of Au Part II. A chemical and structural basis of oxidation of the (111) plane. *J. Electroanal. Chem.* 228:429–453.

24. Ataka, K.I., T. Yotsuyanagi, and M. Osawa. 1996. Potential-dependent reorientation of water molecules at an electrode/electrolyte interface studied by surface-enhanced infrared absorption spectroscopy. *J. Phys. Chem.* 100:10664–10672.

25. Rodríguez, O., M.A. Pence, and J. Rodríguez-López. 2023. Hard Potato: A Python Library to Control Commercial Potentiostats and to Automate Electrochemical Experiments. *Anal. Chem.* 95:4840–4845.

26. Jo, S., T. Kim, V.G. Iyer, and W. Im. 2008. CHARMM-GUI: A web-based graphical user interface for CHARMM. *J. Comput. Chem.* 29:1859–1865.

27. Lee, J., X. Cheng, J.M. Swails, M.S. Yeom, P.K. Eastman, J.A. Lemkul, S. Wei, J. Buckner, J.C. Jeong, Y. Qi, S. Jo, V.S. Pande, D.A. Case, C.L. Brooks, A.D. MacKerell, J.B. Klauda, and W. Im. 2016. CHARMM-GUI Input Generator for NAMD, GROMACS, AMBER, OpenMM, and CHARMM/OpenMM Simulations Using the CHARMM36 Additive Force Field. *J. Chem. Theory Comput.* 12:405–413.

28. Choi, Y.K., N.R. Kern, S. Kim, K. Kanhaiya, Y. Afshar, S.H. Jeon, S. Jo, B.R. Brooks, J. Lee, E.B. Tadmor, H. Heinz, and W. Im. 2022. CHARMM-GUI Nanomaterial Modeler for Modeling and Simulation of Nanomaterial Systems. *J. Chem. Theory Comput.* 18:479–493.

29. Kern, N.R., J. Lee, Y. Kyo Choi, and W. Im. 2022. CHARMM-GUI multicomponent assembler for modeling and simulation of complex multicomponent systems. *Biophys. J.* 121:529a.

30. Huang, J., S. Rauscher, G. Nawrocki, T. Ran, M. Feig, B.L. De Groot, H. Grubmüller, and A.D. MacKerell. 2016. CHARMM36m: An improved force field for folded and intrinsically disordered proteins. *Nat. Methods*. 14:71–73.

31. William, L.J., C. Jayaraman, D.M. Jeffry, W.I. Roger, and L.K. Michael. 1983. Comparison of simple potential functions for simulating liquid water. *J. Chem. Phys.* 79:926–935.

32. Heinz, H., R.A. Vaia, B.L. Farmer, and R.R. Naik. 2008. Accurate simulation of surfaces and interfaces of face-centered cubic metals using 12-6 and 9-6 lennard-jones potentials. *J. Phys. Chem. C*. 112:17281–17290.

33. Thompson, A.P., H.M. Aktulga, R. Berger, D.S. Bolintineanu, W.M. Brown, P.S. Crozier, P.J. in 't Veld, A. Kohlmeyer, S.G. Moore, T.D. Nguyen, R. Shan, M.J. Stevens, J. Tranchida, C. Trott, and S.J. Plimpton. 2022. LAMMPS - a flexible simulation tool for particle-based materials modeling at the atomic, meso, and continuum scales. *Comput. Phys. Commun.* 271:108171.

34. Ahrens-Iwers, L.J.V., M. Janssen, S.R. Tee, and R.H. Meißner. 2022. ELECTRODE: An electrochemistry package for atomistic simulations. *J. Chem. Phys.* 157.

35. Yeh, I.C., and M.L. Berkowitz. 1999. Ewald summation for systems with slab geometry. *J. Chem. Phys.* 111:3155–3162.

36. Shinoda, W., M. Shiga, and M. Mikami. 2004. Rapid estimation of elastic constants by molecular dynamics simulation under constant stress. *Phys. Rev. B - Condens. Matter Mater. Phys.* 69.

475 37. Reed, S.K., O.J. Lanning, and P.A. Madden. 2007. Electrochemical interface between an
476 ionic liquid and a model metallic electrode. *J. Chem. Phys.* 126.

477 38. Dufils, T., G. Jeanmairet, B. Rotenberg, M. Sprik, and M. Salanne. 2019. Simulating
478 Electrochemical Systems by Combining the Finite Field Method with a Constant Potential
479 Electrode. *Phys. Rev. Lett.* 123.

480 39. Tee, S.R., and D.J. Searles. 2022. Fully periodic, computationally efficient constant potential
481 molecular dynamics simulations of ionic liquid supercapacitors. *J. Chem. Phys.* 156.

482 40. Ryckaert, J.P., G. Ciccotti, and H.J.C. Berendsen. 1977. Numerical integration of the
483 cartesian equations of motion of a system with constraints: molecular dynamics of n-alkanes.
484 *J. Comput. Phys.* 23:327–341.

485 41. Ahrens-Iwers, L.J.V., and R.H. Meißner. 2021. Constant potential simulations on a mesh. *J.*
486 *Chem. Phys.* 155.

487 42. Van Der Spoel, D., E. Lindahl, B. Hess, G. Groenhof, A.E. Mark, and H.J.C. Berendsen.
488 2005. GROMACS: Fast, flexible, and free. *J. Comput. Chem.* 26:1701–1718.

489 43. Auer, B., R. Kumar, J.R. Schmidt, and J.L. Skinner. 2007. Hydrogen bonding and Raman,
490 IR, and 2D-IR spectroscopy of dilute HOD in liquid D2O. *Proc. Natl. Acad. Sci. U. S. A.*
491 104:14215–14220.

492 44. Davis, J.G., K.P. Gierszal, P. Wang, and D. Ben-Amotz. 2012. Water structural
493 transformation at molecular hydrophobic interfaces. *Nature*. 491:582–585.

45. Osawa, M., K.I. Ataka, K. Yoshii, and Y. Nishikawa. 1993. Surface-enhanced infrared spectroscopy: The origin of the absorption enhancement and band selection rule in the infrared spectra of molecules adsorbed on fine metal particles. *Appl. Spectrosc.* 47:1497–1502.